Catalysis Today 145 (2009) 63–71

Contents lists available at ScienceDirect

Catalysis Today

journal homepage: www.elsevier.com/locate/cattod

Performances and stability of a Pd-based supported thin film membrane prepared by EPD with a novel seeding procedure. Part 1—Behaviour in H_2:N_2 mixtures☆

Salvatore Abate, Chiara Genovese, Siglinda Perathoner, Gabriele Centi *

Dipartimento di Chimica Industriale ed Ingegneria dei Materiali (INSTM – UdR Messina and ELCASS), University of Messina, Salita Sperone 31, 98166 Messina, Italy

ARTICLE INFO

Article history:
Received 1 February 2008
Received in revised form 18 June 2008
Accepted 19 June 2008
Available online 5 August 2008

Keywords:
Hydrogen separation
Palladium
Membrane
Electroless plating deposition

ABSTRACT

The performances and long-term stability in the 350°–450 °C temperature range of a Pd–Ag alloy thin film membrane are reported. The membrane was prepared by electroless plating deposition (EPD) on the inner walls of a tubular alumina asymmetric support using a novel seeding procedure based on Pd-only complexes. A defect-free film with thickness around 12 microns is obtained. Scanning electron microscopy (SEM) images evidence the presence of aggregates of small crystallites of few hundred nanometers. The membrane shows a stable behaviour for at least 260 h of time-on-stream in pure H_2 and permeability tests indicate a high hydrogen flux with an activation energy of about 14 kJ/mol. The permeability follows Sievert's law with an exponent of 0.5, indicating a bulk diffusion of hydrogen as the rate-controlling step. There is an initial increase in the transmembrane H_2 flux during the time-on-stream tests, due to hydrogen absorption in the Pd–Ag alloy which increases the permeation rate. The presence of two mechanisms of transport, within Pd–Ag alloy crystallites and in the intergrain boundary region, is discussed. The permeability behaviour using H_2:N_2 mixtures as the feed is also shown. The presence of N_2 induces a large decrease in the H_2 permeation rate, greater than that expected by dilution effect. The membrane is stable in the 350°–400 °C temperature range with a high separation factor between H_2 and N_2, but at 450 °C shows an initial fast decrease of the selectivity with time-on-stream up to reach a nearly constant value. The effect is interpreted in terms of formation of NH_x species which inhibit hydrogen diffusion in the intergrain boundary region, as suggested also from literature data.

1. Introduction

The raising request of hydrogen (with a rate of about 10–12% in the last 5 years) for producing cleaner fuels and other applications has renewed the interest on the processes for H_2 production by hydrocarbon reforming. Steam reforming of natural gas is a well-established technology in refining and fertilizer industries for the production of hydrogen [1,2]. After a stage of sulphur removal, there are two consecutive stages, the first of steam reforming and the second of water gas shift to convert CO. The products of reaction are then send typically to a pressure-swing adsorption (PSA) separation unit to eliminate CO_2 and produce H_2 with high purity.

The process requires high temperatures in the range of 850–930 °C and high pressures, 15–40 bar. Due to such operating condition, steam for export is usually produced in order to improve the overall efficiency. The typical methane conversion is 75–80%. Taking into account of the steam credit, the feedstock + fuel requirement is typically in the range of 3200–3500 kcal (LHV)/Nm^3 of hydrogen produced. The use of a membrane-reforming reactor makes possible to push the chemical equilibrium towards conditions favouring hydrogen production, while allowing methane conversion at a temperature lower than 550 °C. Such a low temperature, in turn, will make it possible to locate the membrane reforming reactor downstream of a gas turbine, realizing an efficient hybrid system (power + hydrogen) with a reduction in energy consumption, e.g., with system efficiency around 2700 kcal/Nm^3 H_2 which is significantly better than that of conventional processes [3,4]. There are, thus, not only advantages in the process efficiency and in the reduction of greenhouse gas emissions per ton of H_2 produced, but also improvements in process economics. The fabrication of highly reliable, defect-free and reproducible, membranes for selective hydrogen separation, however, is a key issue in the proposed process architecture. The membranes should have high H_2 flux, but at the same time high permselectivity and stability during operations at temperature around 450–500 °C.

While the largest part of studies consider the direct integration of the membranes in the reforming reactor, the proposed scheme considers separate membrane and reforming units. The advan-

☆ In honor of friend Julian Ross, a scientist which greatly contributed to science of catalysis and advanced nanomaterials.

* Corresponding author. Fax: +39 090 391518.
E-mail address: centi@unime.it (G. Centi).

0920-5861/$ – see front matter © 2008 Elsevier B.V. All rights reserved.
doi:10.1016/j.cattod.2008.06.024

tages are the possibility of better optimization of the reaction temperature in the two units, easier mechanical design and substitution of membranes, and greater flexibility [3,4]. However, the characteristics of the membranes should be different from those of membranes inside the reforming reactor, due to the different operative conditions and constrains.

Palladium membranes have received growing attention for separation and purification of hydrogen, due to the unique permselectivity of palladium to hydrogen and good mechanical stability [5–9]. First patent claims were based on the use of planar-type membranes based on self-supporting Pd-alloy dense films. However, costs and mechanical stability were not found suitable for the application. More recently, the attention was focused on the use of Pd-alloy thin films supported either on a metallic or a ceramic substrate [10–14]. Although more robust, the first class of membranes requires an intermediate ceramic layer between the Pd-alloy thin film and the metallic substrate to limit inter-diffusion effects. However, stability is an issue. Pd-based thin films are preferable from this point of view, even their intrinsic lower mechanical robustness.

The introduction of alloying elements into the palladium membranes has been used to improve their resistance to hydrogen embrittlement [15–20]. The alloying element (Ag, Cu in particular) is typically used in a concentration of around 20% and the presence of these elements is claimed to allow better stability of the membrane, although a lowering of the permeability is observed.

Several methods have been proposed and developed to prepare Pd-based membranes including magnetron sputtering [17,18], spray pyrolysis [16], and chemical vapour deposition [15]. These methods produce very thin films (few microns) which, when deposited on ceramic membranes with the typical roughness and porosity, do not produce defect-free films showing good permeoselectivity and stable performances. For this reason, it is often preferred to prepare these Pd-based thin films by electroless plating deposition (EPD) [10,11,18,19] which typically allows to prepare films having thickness around 10–20 microns which optimize the contrasting factor of film robustness, minimization of defects, selectivity and permeability. However, precise indications on these aspects are limited in literature.

The EPD method involves a first stage of creation of uniformly dispersed Pd-based seeds on the ceramic substrate. These Pd-based nanoparticles act as the centres of decomposition of hydrazine in a second stage. The electrons generated in this reduction process are used to reduce locally Pd^{2+} ions present in the aqueous hydrazine solution and/or other metallic ions, when a Pd-alloy should be produced. There is, thus, a deposition of Pd-based nanocrystals near to the seeds and this accelerates the process of hydrazine decomposition and further reduction of metals. When the process is not carefully controlled, the growing of 3D fractal-like nanostructures of Pd (or Pd-alloy) instead of the deposition of a Pd-based film with uniform thickness is observed. The conditions of plating and the seeding procedure may thus significantly affect the features and performances of the obtained membrane.

Creation of Sn–Pd seed is the typically used procedure for non-conductive substrates. Excess tin remains as colloidal particles, which shield the activated palladium nuclei and remarkably reduce its catalytic activity by inhibiting the hydrogen sorption capability. Namely, incorporation of Sn into the Pd film often results in easy delamination and defect formation due to adhesion loss.

An alternative procedure that eliminates tin contamination on the alumina surface is the impregnation of a palladium complex, followed by reduction with hydrazine. Dip coating and washing of the precursor and successive reduction of palladium with an alkaline hydrazine solution could be used for seeding palladium particles on the substrate:

$$2Pd^{2+} + N_2H_4 + 4OH^- \rightarrow 2Pd^0 + N_2 + 4H_2O \quad (1)$$

There are limited literature data on the effect of seeding procedure on the performances of the membranes. However, we observed that the use of Pd-only seeds instead of Pd–Sn seeds, as typically reported in literature, leads to better membranes. The aim of this work is to study the characteristics, performances and stability of membranes prepared by this novel seeding procedure. In part 1 will be reported the studies using H_2 and H_2:N_2 mixtures. The effect of CO and CO_2 on the performances and stability will be reported in part 2.

2. Experimental

2.1. Preparation of the membranes

Asymmetric porous α-Al_2O_3 tubes provided by INOCERMIC, Germany, were used as the substrate for the deposition of Pd-based thin films. The alumina tube is characterized by a macroporous support (3 μm pore size, about 1.5 mm thickness with a final α-Al_2O_3 mesoporous layer (pore size 70 nm, about 20 microns thickness) on the internal side of the tube. A layer with intermediate porosity and thickness of about 20 microns is present between the two alumina layers. The inner and outer diameters of the tubes were 0.7 and 1.0 cm respectively, and the length of the tube was 13 cm. On the external side of the tube, a ceramic smooth layer is deposited for a length of about 1.5 cm to improve the sealing of the tube in the membrane reactor (Fig. 1).

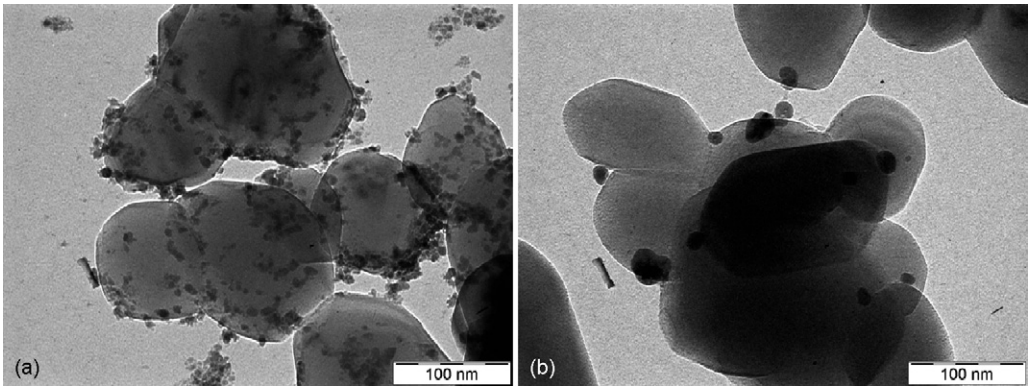

Fig. 1. Transmission electron microscopy images of the Pd-based nanoparticles deposited on alumina by seeding procedure during the EPD method: (a) conventional procedure with deposition of Pd–Sn particles and (b) novel seeding procedure to deposit Pd-only particles.

The ceramic support is first cleaned from grease and other contaminations using purified isopropanol and then dried at 100 °C for 3 h. A thin film of Pd–Ag (23 wt% Ag) was then deposited on these membranes by EPD method. This EPD technique consists of two main consecutive steps: (i) first Pd-based nanocrystals (seeds) are created on the membrane surface (seeding or activation step), and then (ii) deposition of a Pd–Ag layer occurs by reduction of Pd and Ag ions present in an aqueous solution in contact with the inner part of the alumina tube using the electrons generated in the reduction of hydrazine over the Pd-based nanocrystals.

The novel seeding procedure to deposit Pd-nanocrystals on the inner walls of the alumina tube was as follows. Two solutions were prepared. Solution A was an HCl aqueous solution (0.1 N) containing 2 wt% $PdCl_2$. Solution B was an aqueous 2 M solution of hydrazine. The alumina tube, which external side was protected with Parafilm®, was immersed in solution A for 2 min. After washing with distilled water, the tube was then immersed in solution B for 2 min and then washed with distilled water. This cycle was repeated 8 times. The conventional seeding procedure produces a high number of Pd–Sn seeds with dimensions of few nanometers which tend to aggregate each other (Fig. 1a). The novel procedure used in this work gives rise to a reduced number of Pd-only particles having typically larger mean diameter than that of the particles obtained with the conventional procedure (Fig. 1b). However, during the consecutive electroless plating, a better control of the relative rates of nucleation versus crystal growth is possible with a consequent production of less defects and pinholes in the subsequent deposition of the Pd–Ag alloy membrane, at least in the conditions we used for EPD method.

After the seeding with Pd-based nanocrystals, electroless plating of the activated alumina tube was carried out by immersion of the alumina tube into a well-stirred plating bath containing Pd and Ag salts, EDTA, ammonia and hydrazine. The external surface of the alumina-tube was covered with parafilm to prevent plating. The whole system was placed in a thermostated chamber maintained at 50 °C, adding at the same time 1 ml of N_2H_4 (1M) drop wise. The membrane was kept 5 h under stirring and then it was washed with distilled water and dried at 110 °C (2 h). The procedure could be repeated several times in order to increase the thickness of the deposited Pd–Ag film. The chemical composition of the optimized plating bath solution containing both Pd and Ag ions, EDTA, ammonia and hydrazine is given in Table 1. This optimized composition was determined in preliminary tests and used for both types of seeding procedure. The Pd–Ag alloy was finally formed by treating the membrane at 500 °C in N_2 for 5 h. Previously, it was reported on analogous Pd–Ag membranes supported on Al_2O_3, that at this temperature Ag–Pd alloy formation occurs on the hand of XRD experiments [20].

Table 1
Composition of the plating bath in the preparation of membrane

Electroless plating bath of $Pd_{77}Ag_{23}$	
$PdCl_2$	5 g/l
$AgNO_3$	1.24 g/l
EDTA	40 g/l
NH_4OH (25%)	290 ml/l
N_2H_2 (1 M)	10 ml/l
pH	11
Bath temperature	50 °C
Time	5 h
Heating treatment in N_2 (60 ml/min)	5 h at T = 500 °C

2.2. Experimental apparatus

In order to evaluate the permeation behaviour of the Pd/Ag membrane, and the separation performance, the stainless steel reactor (permeator) shown in Fig. 2 was used. Both annular ends between the membrane tube and the permeator wall were sealed with moulded graphite rings. The permeator was placed in an electrical furnace and heated to the desired temperatures (range 350–450 °C). A K-type thermocouple within the membrane tube was used to control the temperature during the permeation experiments. All gases were introduced into the permeator using a calibrated multi-channel mass-flow controller.

The inlet feed was connected to the inner side of the membrane and the permeated gases were measured on the outer side of the membrane, at atmospheric pressure. No sweep gas has been used. The pressure in the inner side of the tube was monitored via a pressure controller.

Before starting with permeability tests, experiments to determine external mass transfer limitations were carried out using different flow rates of H_2.

Permeability data were collected in the 350–450 °C temperature range for pure hydrogen and a hydrogen-nitrogen mixture by varying N_2 composition between 50 and 20%. The inlet flow rate was 18 l/h with pressures on the feed (P_f) side (inner part of the tube) from 1 bar to 5 bar, while the low pressure (permeate) side was maintained at 1 bar (P_p). The stability tests, if not otherwise

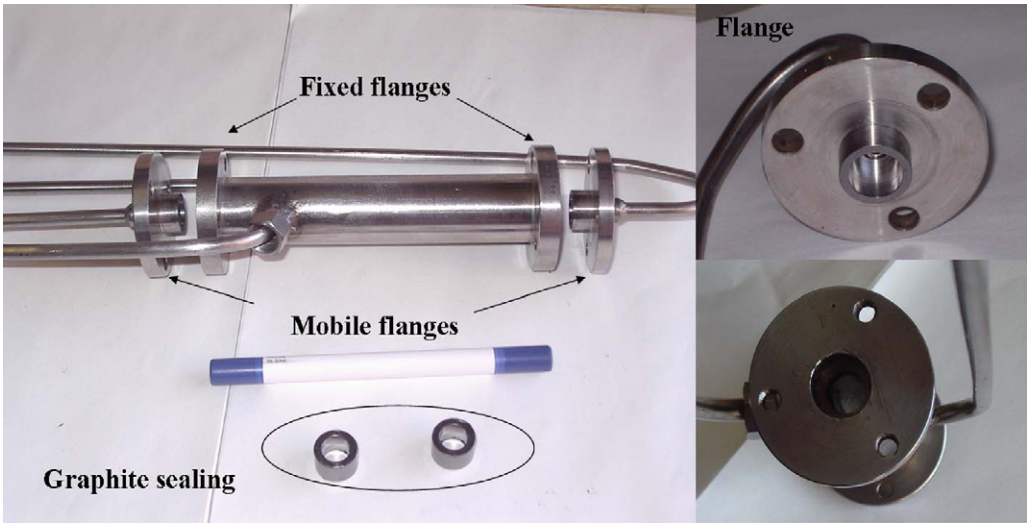

Fig. 2. Stainless steel membrane reactor (permeator) and membrane used in the tests.

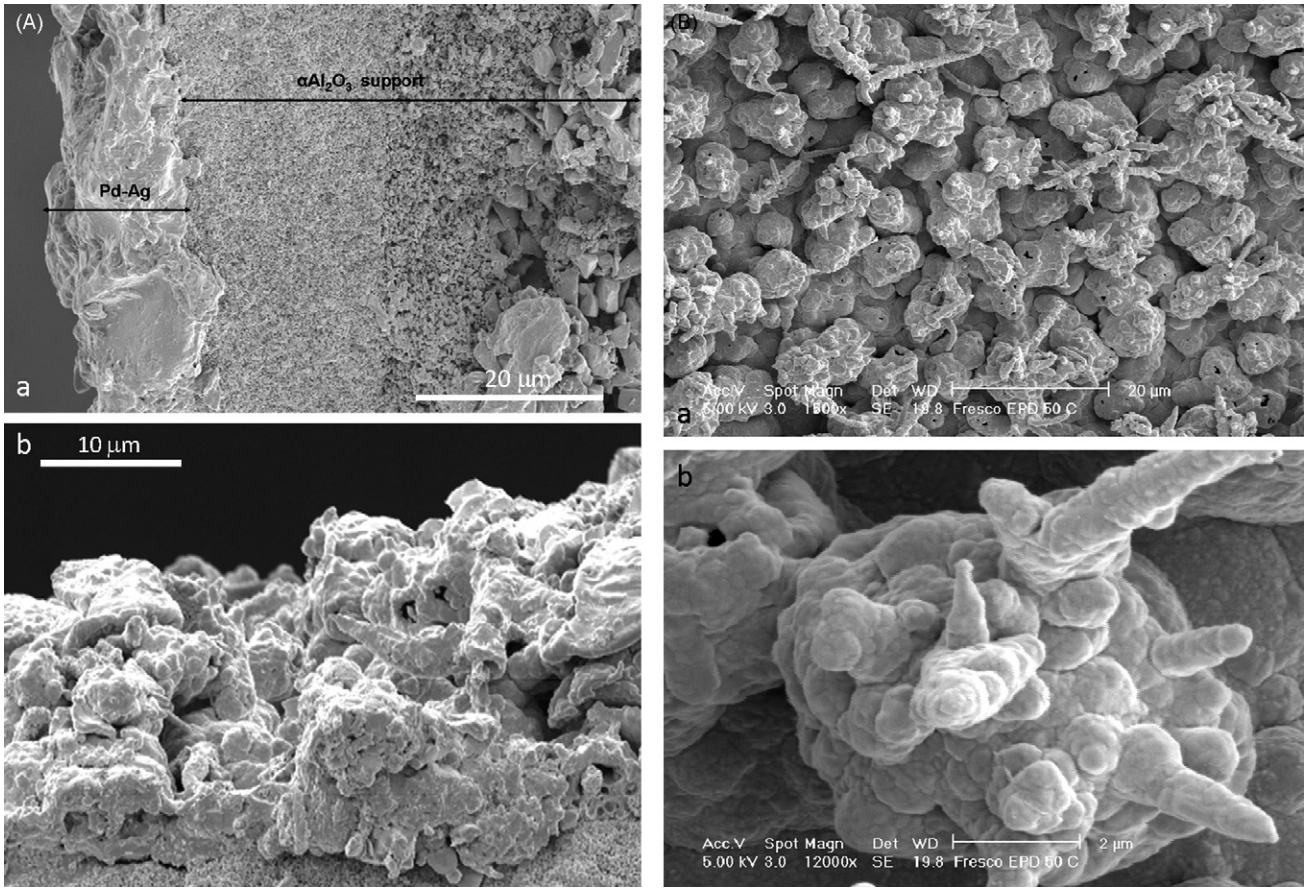

Fig. 3. Scanning electron microscopy (SEM) image of the (A) cross-section and (B) top view of the fresh membrane.

indicated, were made at a P_f of 2 bar. The flow rate of either permeate or feed gas was measured by digital mass flow meters connected to a personal computer. The composition of the feed, permeate and retentate streams were analyzed using a gas chromatograph unit (Agilent 3000 A equipped with a Molsieve 5 Å column using Argon as carrier gas).

2.3. Characterization

EDX–SEM characterization studies of the membranes were made with a scanning electron microscope Jeol 5600LV. Elemental analysis was carried out via energy dispersion analysis using an X-ray analytical system EDX OXFORD, coupled to the scanning electron microscope. The tubular membranes were cut for this characterization.

Leak tests, to analyze both the absence of defects in the membrane and the sealing of the graphite rings, was made by pressuring the membrane with He up to a pressure of 9 bars, e.g., about 1.5 times higher than the maximum pressure used in permeability studies, and immersing the membrane in a ethanol/water mixture.

Transmission electron microscopy (TEM) studies were made on a Philips TEM/STEM CM200 LaB6 apparatus, operating at 200 kV.

3. Results and discussion

3.1. Characterization of the membrane

The scanning electron microscopy images of the cross section of the fresh membrane are reported in Fig. 3A. The mean thickness of the Pd–Ag membrane is around 12 microns and a relatively dense film is present without the appearance of cracks. Leak tests confirmed the absence of detectable defects in the membrane. No apparent segregation of Pd and Ag inside the Pd–Ag layer could be observed by line profile obtained with EDS–SEM method and X-ray diffraction indicates the presence of a Pd–Ag alloy.

A significant surface roughness is present (some microns), which reflects the roughness of the underlying α-Al_2O_3 layer with mean porosity diameter of 70 nm. The asymmetric nature of the alumina tube, formed by three layers with decreasing porosity, could be also observed (Fig. 3Aa). However, the surface roughness of the underlying alumina substrate is necessary to guarantee a good mechanical stability of the Pd–Ag membrane and avoid the delamination and/or formation of cracks during operations. Tests changing the porosity and surface roughness of the final ceramic layer confirmed the relevance of this factor to prepare stable membranes.

The micromorphology of the Pd–Ag film is characterized from the presence of irregular macrodomains with dimension of few microns which are formed by an assembly of smoothed nanoparticles of 100–200 nm (Fig. 3B). Some rod-like macro-structures with length up to 20 microns and diameter in the 200–500 nm range could be observed, but the prevalent macrocrystallite morphology is cauliflower-like which was observed also in other membranes prepared by the EPD method [10,11,18,19]. Few holes could be apparently detected in the top-view of the membrane (Fig. 3B), but the cross section shows that these holes do not cross the membrane (Fig. 3A), in agreement with leak tests which do not provide evidence of the presence of pinholes.

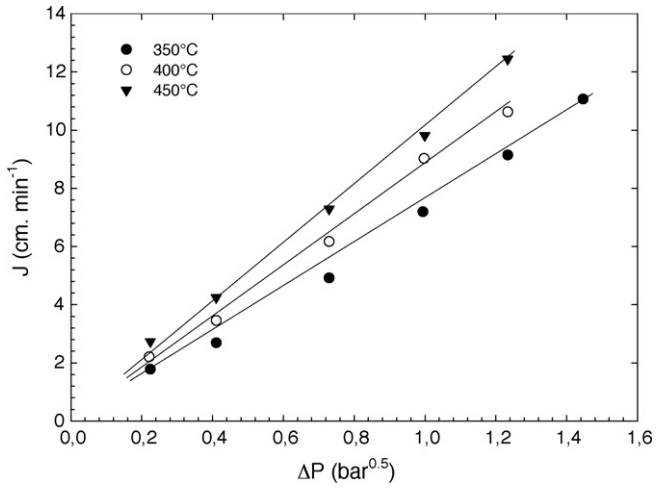

Fig. 4. Relationship between hydrogen permeation flux and the difference in the square root of hydrogen pressure between the tube-side and the shell-side (ΔP) at different temperatures.

3.2. Permeability tests

The permeation behaviour of the membrane was measured with pure H_2 at three different temperatures in the 350–450 °C range. The results are reported in Fig. 4. Tests were made analyzing the H_2 permeate flux as a function of time at a fixed temperature and transmembrane pressure differential. A stable behaviour is typically observed after few hours, but in some cases the time of the test was extended to have better indications on stability of operations. Then the pressure differential across the membrane is increased (ΔP in the 0.5–5 bar range) and the flux of H_2 monitored again as a function of time-on-stream. Fig. 5a shows the sequence of experiments at 350 °C. After completing the measurements, the ΔP was decreased to 0.5 and the temperature raised. After stabilization, a new series of tests at the higher temperature was made.

Fig. 5b shows a summary of the sequence of tests. It can be observed an initial increase in the permeate rate, due to absorption of hydrogen in the Pd–Ag membrane which causes an expansion of the lattice. In fact, the atomic distance between Pd atoms increase from 0.389 nm to 0.403 nm, when chemisorbed H/Pd ratio increases from 0.06 to 0.6 [21,22]. In separate thermogravimetric tests, the increase of weight of Pd–Al alloy membrane was confirmed. After this initial increase of the rate of hydrogen permeation, a constant permeate rate of H_2 was observed in all the studied range of temperatures (Fig. 5b). Total time of these experiments was over 260 h (Fig. 5b), indicating the good stability of the membrane. A reproducibility of the initial results was also observed decreasing back the reaction temperature and pressure differential across the membrane after the tests at the higher temperature and pressure.

The results reported in Fig. 4 indicate that the permeation rate of H_2 is directly proportional to $\Delta P = P_f^{0.5} - P_p^{0.5}$, e.g. the difference in the square roots of hydrogen pressures between the feed (f) and the permeation (p) sides of the membrane. This is consistent with Sievert's law [23] for defect-free membranes:

$$J_{H_2} = \frac{Q}{\delta}(P_f^n - P_p^n) \quad (2)$$

where J_{H_2} is the transmembrane flux of H_2, Q the permeability and δ the thickness of the Pd–Ag membrane. The exponent n varies between 0.5, when the rate-limiting step is the bulk transport of hydrogen across the membrane, to 1.0, when the surface dissociation of hydrogen is the limiting step [14,24].

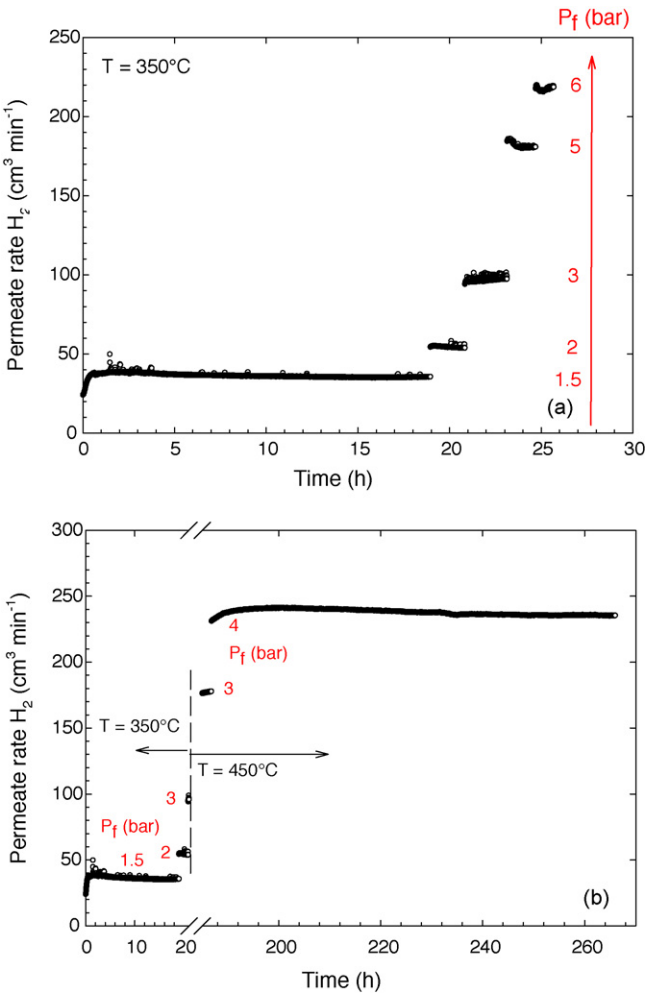

Fig. 5. Permeate rate of H_2 versus time-on-stream during the experiments to study the permeability of the membrane: (a) effect of the partial pressure on the feed side (P_f) at 350 °C and (b) summary of the sequence of tests at different temperatures and pressures.

The good linearity and fitting of the data using a value of $n = 0.5$ indicates a pinholes-free membrane in our case. In fact, when defects and pinholes are present (including when sealing of the membrane at the ends is not perfect), hydrogen could permeate also by Knudsen diffusion and Poiseuille flow which induce deviations from the linearity observed in Sievert's law. In addition, the value 0.5 for n indicates that the rate-determining step is the bulk transport of hydrogen across the membrane. Often higher values of n have been reported in literature [25–28].

The Q/δ is the permeance which can be obtained from linear regression of the data reported in Fig. 4. Table 2 summarizes the dependence of the permeance from the reaction temperature. The

Table 2
Permeance as a function of the temperature for fresh membrane and values of R^2 in linear regression of the data reported in Fig. 4

T, °C	$Q/\Delta z$ (cm min^{-1} bar$^{-0.5}$)	R^2 (from linear regression)
350	7.38	0.9925
400	8.70	0.9945
450	10.05	0.9947

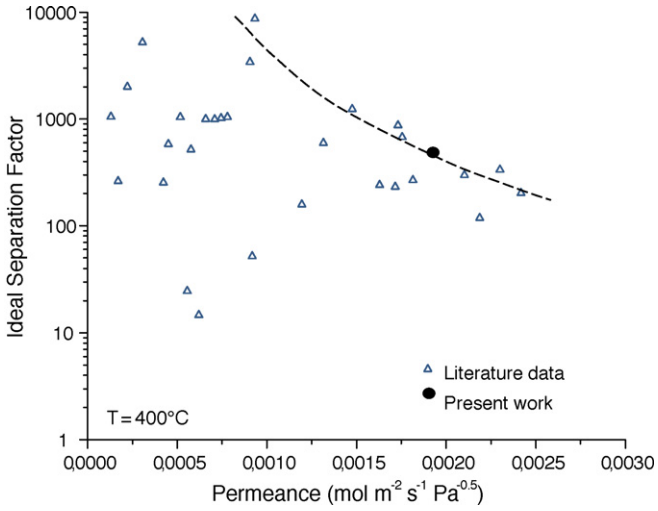

Fig. 6. Comparison of the behaviour of the membrane studied in this work with the data on Pd-based membranes reported by Nair and Harold [29] (see the work of Nair and Harold for the reference to published literature results included in their comparison graph).

values of the R^2 obtained during the linear regression are also reported, which give an indication of the good fitting of the data.

The comparison of the results on permeability with literature data is difficult due to the wide range of reaction conditions used as well as membrane characteristics, which makes often not homogeneous the comparison. Recently Nair and Harold [29] published a comparison of their results on new supported Pd membranes with high permeation characteristics with a number of homogeneous literature data and observed a kind of limiting curve between separation factor (in 50:50 H_2–N_2) mixture and H_2 permeance at 400 °C. Fig. 6 compares the behaviour of the membrane reported in the present study with all the results reported by these authors [29] (their and literature results) in similar reaction conditions. This comparison indicates that the performances of our membrane are close to the optimal values reported in literature.

The experimental value of H_2 permeance (Q/δ) at different temperatures were used to estimate the activation energy for H_2 permeation, using an Arrhenius plot. The results are reported in Fig. 7. A linear fit of the data gives a value of the regression coefficient (R^2) of 0.9994 which further confirm the validity of considerations reported above. The activation energy of the Pd–Ag

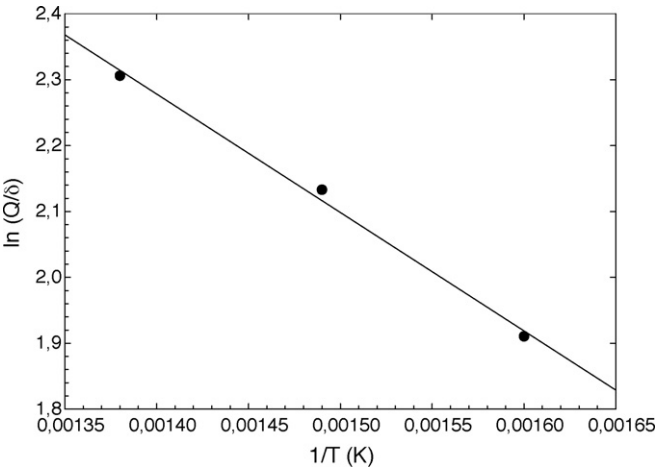

Fig. 7. Arrhenius plot of the relationship between the H_2 permeance and temperature in a fresh membrane.

membrane was found to be 14.68 kJ/mol, which was close to the values previously reported for defect-free Pd membranes.

Mardilovich et al. [30] reported a value of 16.4 kJ/mol, while Collins and Way [31] a value of 14.5 kJ/mol for a Pd film of 17 microns on a ceramic support. Activation energies around 15–16 kJ/mol have been reported also by Kaliaguine and co-workers [14] for hydrogen permeation through tick palladium films, while Matsumura and co-workers [25] reported much higher values for very thin films, e.g. 30.8 kJ/mol for a 3 microns Pd-only film and 25.7 kJ/mol for a 3 microns Pd film on which a further 2 microns $Pd_{0.8}Ag0_{.2}$ alloy layer was electroplated. In the latter samples, however, the n exponential in the Sievert's law (Eq. (2)) was close to one, indicating that surface dissociation of hydrogen is the rate-controlling step. It is, thus, reasonable to observe in these samples a higher activation energy for H_2 permeation.

Lower values of the activation energy have been also reported. Kaliaguine and co-workers [32] and Lu and co-workers [33] reported a value of about 8.3 kJ/mol, and even lower values have been reported (2.2 kJ/mol [34] and about 6 kJ/mol [35,36]. There is, thus, great inconsistency for activation energy data in literature, even if it should be observed that values below about 10 kJ/mol are not consistent with a mechanism of bulk transport of hydrogen through a Pd membrane, but with a prevailing Knudsen diffusion in micropores.

Dannetun and co-workers [35] studying the behaviour of Pd and $Pd_{70}Ag_{30}$ membranes at temperatures below and above 200 °C observed a change in the activation energy. More recently Suzuki and co-workers [37] studied the hydrogen permeability in thin Pd–Ag alloy membranes in the temperature range across the α–β phase transition of palladium hydride (around 170–200 °C). They observed a significant increase in the activation energy and in hydrogen permeation across this transition, because the lattice parameter of β phase (0.403 nm) for pure palladium is 3.4% larger than that of the α phase (0.389 nm). However, in Pd–Ag alloy the differences between α and β phases is minimal (0.13%) [38] and this reduces the difference in the activation energy of hydrogen permeability at temperatures below or above about 200 °C. This result indicates that in pinhole-free samples exists an inverse relationship between rate of hydrogen permeability and activation energy, e.g. when the hydrogen permeation rate is higher, due to a more expanded structure of the Pd-based membrane, the activation energy is lower.

Varma and co-workers [39] studying Pd membranes prepared by electroless plating observed that the activation energy decreases by reducing the mean size of the Pd grains. This suggests that the H diffusion through the membrane occurs both at the grain boundary between the Pd crystals and within the crystals itself. There are limited studies on this aspect, but Ward and Dao [40] modeling the hydrogen permeation behaviour in palladium membranes evidenced that grain boundaries can provide a parallel interstitial diffusion pathway. Fedorov and co-workers [41] also evidenced the role of microstructure on hydrogen permeation in Pd–Ag alloy membranes. The role of intragranular resistance associated with diffusion of H through the bulk of $Pd_{75}Cu_{25}$ alloy membrane was indicated by first-principle's calculations [42].

It may be, thus, tentatively suggested that the large variation observed in literature in the activation energies is not only related to changes in the rate limiting step (from bulk diffusion to surface reaction), but also to the presence of two mechanisms of transport across a defect-free membrane. The first is the diffusion of hydrogen atoms within metal particles and the second in the region at the grain boundaries. The latter is depending on Pd or Pd-alloy nanocrystal sizes, but also to a number of other factors such as presence of dopants, impurities and other elements which accumulate in this region. The first mechanism is influenced from

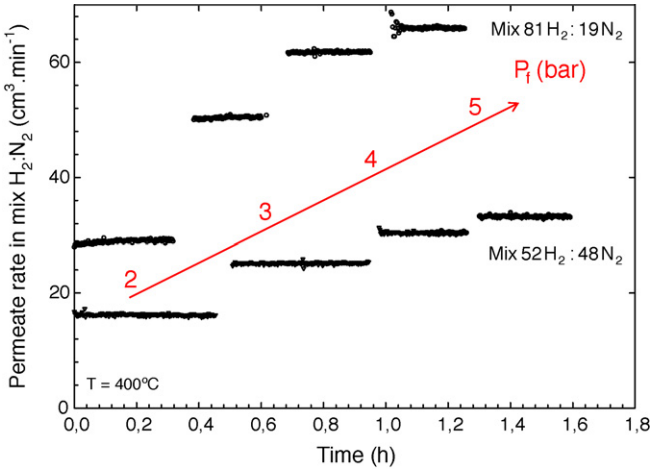

Fig. 8. Permeate rate at 400 °C as a function of time-on-stream in tests using two different H_2:N_2 compositions in the feed and different pressures on feed side (P_f).

the amount of H dissolved, presence of microstrains, type of alloy, etc. There are, thus, many factors which typically are less considered and which explain the very large range of published permeabilities and activation energies for H transport in Pd or Pd-alloy membranes [43–45].

In our case, the value of the activation energy suggests the presence of small grains and a prevalent mechanism of hydrogen transport at the grain boundaries. This indication is consistent with the comparison of SEM images with those earlier reported. The small Pd-based crystals is reasonably associated to the specific modality of preparation and to the use of a different seeding procedure with respect to that typically reported for Pd-based membranes prepared by the EPD method.

3.3. Effect of N_2 on permeability

Fig. 8 reports the flux of permeate at 400 °C as a function of time-on-stream in tests using two different H_2:N_2 compositions in the feed and different pressures on the feed side (P_f). In general, the permeate flux is much lower than in tests using pure H_2 (Fig. 5). However, not only an effect of dilution is present, due to a decrease of the H_2 partial pressure, as usually indicated in literature. In fact, for example in the tests using the $52H_2$:$48N_2$ feed composition, the permeate rate at P_f = 4 bar is about 30 cm^3/min. In tests at 400 °C using pure H_2 and a P_f = 2 bar, e.g. at equal H_2 partial pressure, the permeate rate was about 86 cm^3/min. Using a $81H_2$:$19N_2$ feed, a permeate value of about 43 cm^3/min for a P_f about 2.5 bar, e.g. a partial pressure of H_2 in the feed of about 2 bar, may be extrapolated from the data in Fig. 8. Note that in these tests, the concentration of N_2 in the permeate side is always less that 0.1% and thus do not affect the results. In addition, even for the $52H_2$:$48N_2$ feed, the inlet flow rate of H_2 is about one order of magnitude higher than the permeate rate, e.g. axial concentration gradients along the membrane could be considered negligible.

There is, thus, a specific inhibition effect of N_2 on the flux of H_2 through the membrane. It should be also observed that in these tests, where the flux is monitored for less than 30 min at each pressure in the feed, the permeation rate appears to be constant (Fig. 8).

The relationships between permeate flux and the difference in the square root of pressure between the tube-side and the shell-side (ΔP) at different temperatures using two different compositions in H_2:N_2 binary mixtures in the feed are shown in Fig. 9. It may be noted a general deviation from the linearity observed in tests using pure H_2 (Fig. 4). In particular, a clear deviation for the

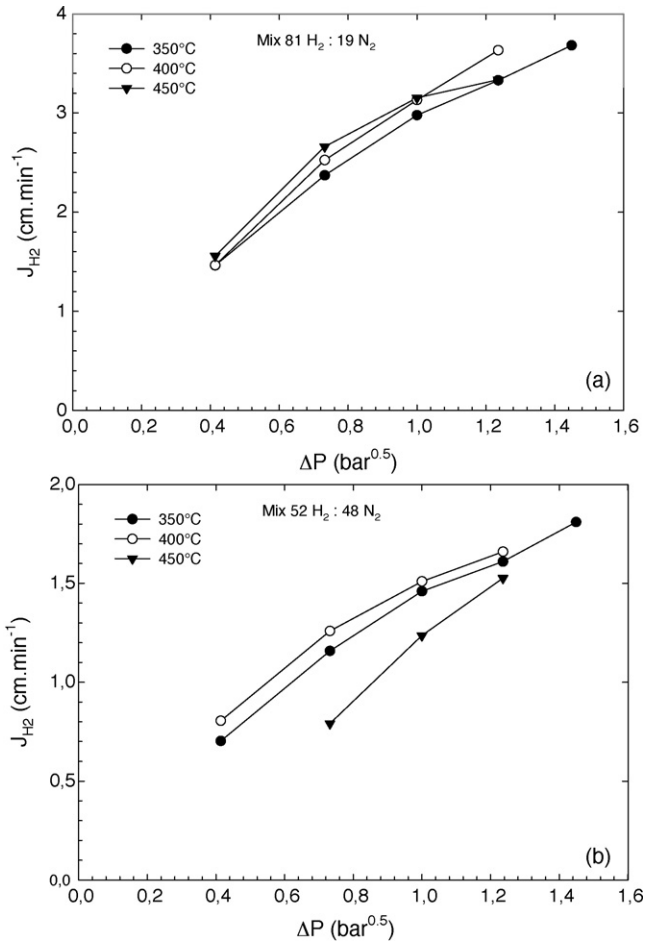

Fig. 9. Relationship between the permeate flux and the difference in the square root of pressure between the tube-side and the shell-side (ΔP) at different temperature using H_2:N_2 binary mixtures in the feed: (a) $81H_2$:$19N_2$, (b) $52H_2$:$48N_2$.

higher pressures in the feed is observed, e.g. higher ΔP. It could be noted also that deviations are more relevant increasing the concentration of N_2 in the feed.

Due to these deviations, the activation energy cannot be estimated correctly. In fact, for the $81H_2$:$19N_2$ mixture, the permeate rate increases with the reaction temperature for ΔP lower than about 1.0, but not for higher pressures. For the $52H_2$:$48N_2$ feed, the permeate rate at 450 °C is lower than at lower reaction temperatures. This further evidences that the presence of N_2 modifies the performances of membranes and that this effect is proportional to the N_2 partial pressure.

Fig. 10 reports the separation coefficient (S_C) calculated in the tests reported in Fig. 9. The separation coefficient S_C was estimated using the following equation:

$$S_{C_{H_2-N_2}} = \frac{J^p_{H_2}/J^p_{N_2}}{J^f_{H_2}/J^f_{N_2}} \quad (3)$$

where J is the flux of H_2 or N_2 on the permeate (p) or feed (f) sides. Note that, often in literature, the simple ratio of H_2 and N_2 fluxes in the permeate side is reported as the separation factor (indicated by Mardilovich et al. [30] as ideal separation factor). The use of the ideal separation factor allows to report higher apparent efficiencies of the membranes, but with values which depend on the composition of the feed. For example, using the $81H_2$:$19N_2$ mixture, an S_C value of about 400 corresponds to an ideal separation factor of about 1700. For a $52H_2$:$48N_2$ mixture, an S_C

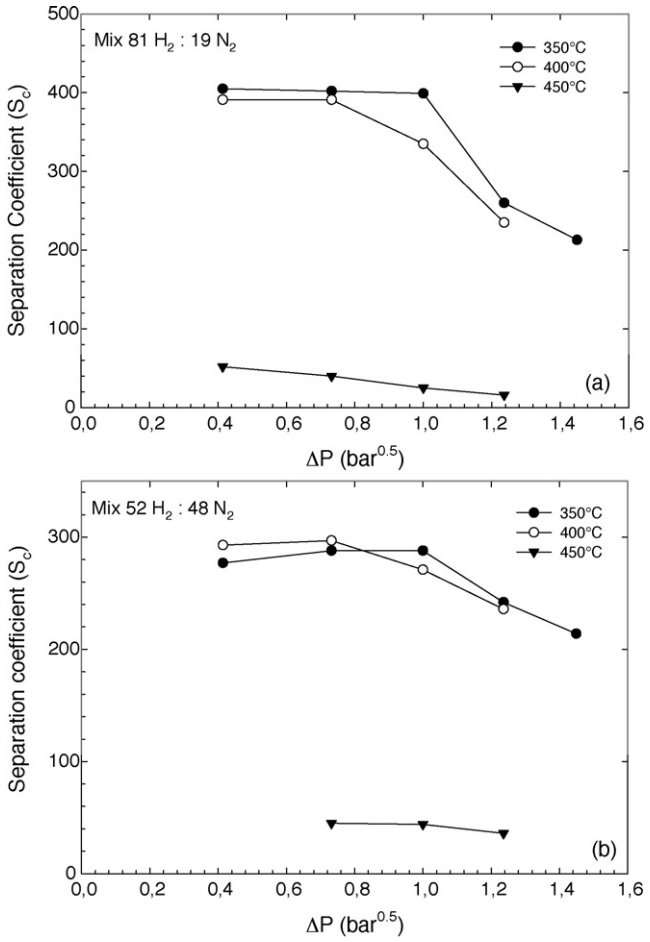

Fig. 10. Relationship between separation coefficient (S_C) and the difference in the square root of pressure between the tube-side and the shell-side (ΔP) at different temperature using H_2:N_2 binary mixtures in the feed: (a) $81H_2$:$19N_2$, (b) $52H_2$:$48N_2$.

value of about 400 corresponds to an ideal separation factor of about 450.

Fig. 10 indicates that the separation factor for a $81H_2$:$19N_2$ feed is around 400 up to a ΔP of about 1.0 in the 350°–400 °C range and decreases at higher pressure and reaction temperatures. For the $52H_2$:$48N_2$ feed, the overall results are similar but the separation factor at the lower temperatures/pressures is about 300. To note the drastic decrease of the separation factor for both feed mixtures in passing from 400 °C to 450 °C, which indicates that nitrogen induces a deactivation of the membrane.

Fig. 11 reports the stability tests of the membrane in the $81H_2$:$19N_2$ feed and $P_f = 2$ bar. In the 350–400 °C temperature range a quite stable separation coefficient (S_C) and permeate flux is observed, while at 450 °C a fast deactivation with the S_C is observed, which decreases from about 250 to 15–20 in about 10–15 h. After these tests at 450 °C, the temperature was decreased to 400 °C again and the behaviour monitored as a function of time-on-stream. After an initial induction time, the separation coefficient increases up to a nearly constant value of 200. This result clearly evidences that the modification induced by nitrogen is reversible, at least partially.

Fig. 12 reports the flow rate of H_2 and N_2 (permeate side) during the tests at 450 °C in the $81H_2$:$19N_2$ feed and $P_f = 2$ bar and consecutive tests at 400 °C. The results show that the change of selectivity is due to a variation in the flux of N_2, while the flux of H_2 remains nearly constant.

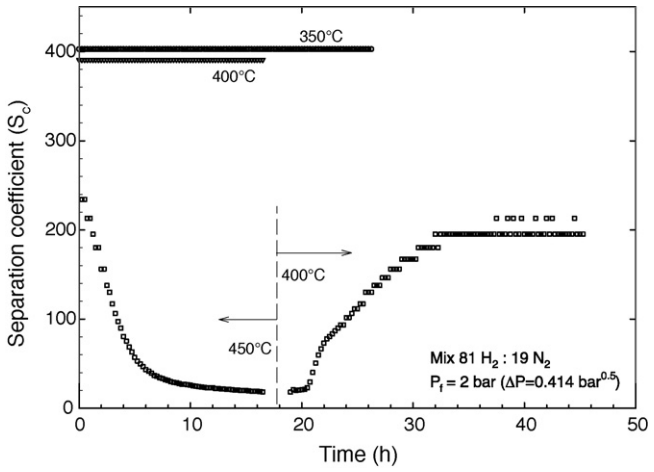

Fig. 11. Separation coefficient (S_C) as a function of time-on-stream in stability tests at 350 °C, 400 °C and 450 °C. Feed: $81H_2$:$19H_2$, $P_f = 2$ bar.

There are very limited studies in literature on the effect of the H_2:N_2 ratio on the stability of Pd-based membranes for H_2 separation, because nitrogen is typically considered an inert gas. However, quite recently Xiong and co-workers [46] have reported a specific investigation on the effect of co-existing nitrogen on hydrogen permeation through thin Pd composite membranes. They observed that the H_2 permeation flux considerably decreases with time-on-stream using an equimolar H_2/N_2 feed and a reaction temperature of 400 °C. No indications, however, are given regarding the separation factor.

Xiong and co-workers [46] observed also that the deactivated membrane could be regenerated in H_2 at temperatures above 450 °C. At 500 °C deactivated membranes could be completely regenerated. They also observed that the use of pure N_2 do not causes deactivation, differently from H_2:N_2 mixtures.

Our data are not fully consistent with those of Xiong and co-workers [46], because the results at a $P_f = 2$ bar (Figs. 11 and 12) do not show a significant change in the permeate flow rate, but rather of the separation factor due to an increase in the nitrogen flux on the permeate side. However, at higher pressures and temperatures, we observed also a decrease in the H_2 transmembrane flux (Fig. 9).

Xiong and co-workers [46] speculated that the inhibition effect of co-existing nitrogen on hydrogen permeation through membranes is due to the blocking of the effective area on the Pd surface for hydrogen diffusion by forming NH_x ($x = 0.2$) species. They also

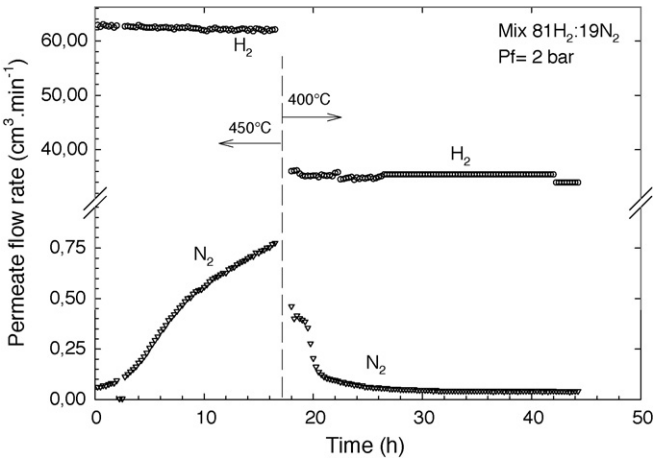

Fig. 12. Permeate flow rate of H_2 and N_2 during tests at 450 °C followed by tests at 400 °C. Other reaction conditions as in Fig. 11.

indicated that these NH_x species are only on the surface and do not diffuse through the membrane.

Our data confirmed that N_2 in the presence of H_2 is not an inert gas and influences the membrane performances even in conditions of bulk transport as the rate determining step, and that the influence of N_2 is reversible. It is reasonable to assume that NH_x-type species could be formed, although other mechanisms could be possible such as the formation of sub-surface N atoms especially in the Pd nanocrystallite grain-boundary region. Nitrogen is considerate insoluble in Pd, but recent data showed that N atoms can diffuse in a Pd film [47]. Differently from Xiong and co-workers [46], we observed that nitrogen could diffuse through the membrane at the higher temperatures and pressures, but the process is slow and a longer time is necessary to establish the same result as that of hydrogen diffusion. We do not observe the presence of ammonia in the permeate side, although detection is difficult, due to the eventually low concentration. On the other hand, we observed the presence of N_2 in the permeate side and it is unlikely that nitrogen diffuses as NH_x species which then dissociates on the permeate side of the membrane to form N_2. It is thus more reasonable to either consider that nitrogen could also diffuse as atomic species in a parallel mechanism to that for *H* transport through the membrane. NH_x species could be also formed, but these are probably responsible of a reversible modification of the properties of the membrane, for example the inhibition of hydrogen transport in the grain-boundary region. The effect of N_2 on membrane performances is thus probably more complex than that indicated by Xiong and co-workers [46], but further studies are necessary for an understanding of the effect. However, the results of this study confirm the indication that N_2 in the presence of H_2 cannot be considered an inert gas.

Acknowledgements

This work has been realized in the frame of the FISR MIUR project "H_2 puro da gas naturale mediante reforming a conversione totale ottenuta integrando reazione chimica e separazione a membrana". The authors wish also to thank Daniele Cosio for the technical assistance in the construction of the reactor and apparatus for membrane tests.

References

[1] G. Shumake, T. Abudiab, Hydrocarbon Eng. 11 (2006) 43.
[2] J.N. Armor, Catal. Lett. 101 (2005) 131.
[3] http://www.fisrproject.com.
[4] (a) S. Abate, G. Centi, S. Perathoner, C. Genovese, G. Iaquaniello, E. Lollobattista, Europacat 8, Turku (Finland), Aug. 2007.;
(b) Ibidem, ACS 235 (New Orleans, April 2008), Div. Petroleum Chemistry (Prepr. Pap.-Am. Chem. Soc., Div. Pet. Chem. 2007, 51 (1&2)).
[5] V.M. Gryaznov, V.M. Ermilova, L.S. Morozova, N.V. Orekhova, et al. J. Less-Common Met. 89 (1983) 529.
[6] N. Itoh, AIChE J. 33 (9) (1987) 1576.
[7] R. Govind, D. Atnoor, IEC Res. 30 (1991) 591.
[8] E. Gobina, R. Hughes, J. Membr. Sci. 90 (1994) 11.
[9] N.N. Mikhalenko, E.V. Khranova, V.M. Gryazanov, Russ. J. Phys. Chem. 59 (1985) 1533.
[10] J. Shu, B.P.A. Grandjean, S. Kaliaguine, Appl. Catal. A 119 (1994) 305.
[11] J. Shu, B.P.A. Grandjean, S. Kaliaguine, Catal. Today 25 (1995) 327.
[12] Z.D. Ziaka, R.G. Minet, T.T. Tsotsis, J. Membr. Sci. 77 (1993) 221.
[13] R.E. Buxbaum, T.L. Marker, J. Membr. Sci. 85 (1993) 29.
[14] J. Shu, B.P.A. Grandjean, A. van Neste, S. Kaliaguine, Can. J. Chem. Eng. 69 (1991) 1036.
[15] S. Yam, H. Maeda, K. Kusakabe, S. Morooka, IEC Res. 33 (1994) 616.
[16] Z.Y. Li, H. Maeda, K. Kusakabe, S. Morooka, H. Anzai, S. Akiyama, J. Membr. Sci. 78 (1993) 247.
[17] V. Jayaraman, Y.S. Lin, M. Pakals, R.Y. Lin, J. Membr. Sci. 99 (1995) 89.
[18] S. Uemiya, N. Sato, H. Ando, Y. Kude, T. Matsuda, K. Kikuchi, J. Membr. Sci. 56 (1991) 303.
[19] S. Abate, G. Centi, S. Melada, S. Perathoner, F. Pinna, G. Strukul, Catal. Today 104 (2005) 323.
[20] S. Abate, G. Centi, S. Perathoner, F. Frusteri, Catal. Today 118 (2006) 189.
[21] F.A. Lewis, The Palladium Hydrogen System, Academic Press, London, 1967, pp. 318.
[22] M. Krukowski, B. Baranowski, J. Less Common Metals 49 (1976) 385.
[23] G.L. Holleck, J. Phys. Chem. 74 (3) (1970) 503.
[24] R. Dittmeyer, V. Höllein, K. Daub, J. Molec. Catal. A 173 (2001) 135.
[25] J. Tong, R. Shirai, Y. Kashima, Y. Matsumura, J. Membr. Sci. 260 (2005) 84.
[26] S.-E. Nam, K.H. Lee, IEC Res. 44 (2005) 100.
[27] B.A. Wilhite, M.A. Schmidt, K.F. Jensen, IEC Res. 43 (2004) 7083.
[28] A.L. Li, W. Liang, R. Hugher, Catal. Today 56 (2000) 45.
[29] B.K.R. Nair, M.P. Harold, J. Membr. Sci. 290 (2007) 182.
[30] P.P. Mardilovich, Y. She, Y.H. Ma, M.H. Rei, AIChE J. 44 (1998) 310.
[31] J.P. Collins, J.D. Way, IEC Res. 32 (1993) 3006.
[32] J. Shu, B.E.W. Bongondo, B.P.A. Grandjean, A. Adnot, S. Kaliaguine, Surf. Sci. 291 (1993) 129.
[33] Y. Guo, G. Lu, Y. Wang, R. Wang, Sep. Purif. Techn. 32 (2003) 271.
[34] J.K. Ali, E.J. Newson, D.W.T. Rippin, J. Membr. Sci. 153 (2000) 269.
[35] H. Amandusson, L.G. Ekedahl, H. Dannetun, J. Membr. Sci. 193 (2001) 35.
[36] E. Serra, M. Kemali, A. Perujo, D.K. Ross, Metall. Mater. Trans. 29A (1998) 1023.
[37] J. Okazaki, D.A.P. Tanaka, M.A.L. Tanco, Y. Wakui, F. Mizukami, T.M. Suzuki, J. Membr. Sci. 282 (2006) 370.
[38] S.D. Axelrod, A.C. Makrides, J. Phys. Chem. 68 (1964) 2154.
[39] R.S. Souleimanova, A.S. Mukasyan, A. Varma, AIChE J. 48 (2002) 262.
[40] T.L. Ward, T. Dao, J. Membr. Sci. 53 (1999) 211.
[41] L.S. McLeod, F.L. Degertekin, A.G. Fedorov, Appl. Phys. Lett. 90 (2007), 261905.
[42] C. Ling, D.S. Sholl, J. Membr. Sci. 303 (2007) 162.
[43] G.Q. Lu, J.C. Diniz da Costa, M. Duke, S. Giessler, R. Socolow, R.H. Williams, T. Kreutz, J. Coll. Interf. Sci. 314 (2007) 589.
[44] S. Adhikari, S. Fernando, IEC Res. 45 (2006) 875.
[45] T.M. Nenoff, R.J. Spontak, C.M. Aberg, MRS Bull. 31 (2006) 735.
[46] W. Wang, X. Pan, X. Zhang, W. Yang, G. Xiong, Separ. Purif. Techn. 54 (2007) 271.
[47] (a) L. Du, S. Ahat, M. Sheng, Z. Sun, W. Huang, L. Luo, J. Mater. Sci. Lett. 20 (2001) 911;
(b) L. Du, S. Ahat, M. Sheng, L. Luo, J. Freytag, W. Senske, J. Alloys Compd. 311 (2000) 270.